Galaxies point at each other and mess up measurements of the Universe

~~Intrinsic Alignment as an RSD Contaminant in the DESI Survey~~

Claire Lamman[1*], Daniel Eisenstein[1], Jessica Nicole Aguilar[2], David Brooks[3], Axel de la Macorra[4], Peter Doel[3], Andreu Font-Ribera[5], Satya Gontcho A Gontcho[2], Klaus Honscheid[6,7], Robert Kehoe[8], Theodore Kisner[2], Anthony Kremin[2], Martin Landriau[2], Michael Levi[2], Ramon Miquel[5,9], John Moustakas[10], Nathalie Palanque-Delabrouille[2,11], Claire Poppett[2,12,13], Michael Schubnell[14,15], Gregory Tarlé[15]

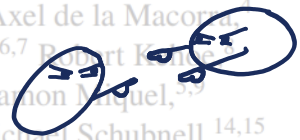

[1]Center for Astrophysics | Harvard & Smithsonian, 60 Garden Street, Cambridge, MA 02138, USA
[2]Lawrence Berkeley National Laboratory, 1 Cyclotron Road, Berkeley, CA 94720, USA
[3]Department of Physics & Astronomy, University College London, Gower Street, London, WC1E 6BT, UK
[4]Instituto de Física, Universidad Nacional Autónoma de México, Cd. de México C.P. 04510, México
[5]Institut de Física d'Altes Energies (IFAE), The Barcelona Institute of Science and Technology, Campus UAB, 08193 Bellaterra Barcelona, Spain
[6]Center for Cosmology and AstroParticle Physics, The Ohio State University, 191 West Woodruff Avenue, Columbus, OH 43210, USA
[7]Department of Physics, The Ohio State University, 191 West 18th Avenue, Columbus, OH 43210, USA
[8]Department of Physics, Southern Methodist University, 3215 Daniel Avenue, Dallas, TX 75275, USA
[9]Institució Catalana de Recerca i Estudis Avançats, Passeig de Lluís Companys, 23, 08010 Barcelona, Spain
[10]Department of Physics and Astronomy, Siena College, 515 Loudon Road, Loudonville, NY 12211, USA
[11]IRFU, CEA, Université Paris-Saclay, F-91191 Gif-sur-Yvette, France
[12]Space Sciences Laboratory, University of California, Berkeley, 7 Gauss Way, Berkeley, CA 94720, USA
[13]University of California, Berkeley, 110 Sproul Hall #5800 Berkeley, CA 94720, USA
[14]Department of Physics, University of Michigan, Ann Arbor, MI 48109, USA
[15]University of Michigan, Ann Arbor, MI 48109, USA

This work uses data that a lot of people all over the world helped with!

Accepted XXX. Received YYY; in original form ZZZ

INFORMATION-DENSE SUMMARY

We measure how the orientations of galaxies correlate with large structures of matter in the Universe. DESI is surveying galaxies, but there is a bias in the orientations of galaxies they choose to observe. We also estimate this bias, and explore how these two effects combine to mess up DESI's measurements of how matter is distributed on large scales (don't worry if this effect isn't immediately obvious!).

Key words: methods: data analysis –cosmology: observations – large-scale structure of Universe – – cosmology: dark energy

INTRODUCTION

The Universe is like old milk. It started out smooth and uniform, but gets clumpier over time.

By measuring the structure of mass clumps and how it changes, we learn about the components which create it –i.e. gravity and dark energy.

DESI is doing this by mapping out 40 MILLION galaxies. To make the best use of all this data and get the most accurate measurements possible, we need to understand even the smallest sources of error.

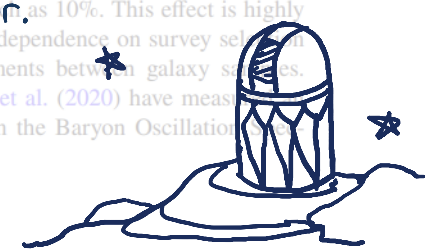

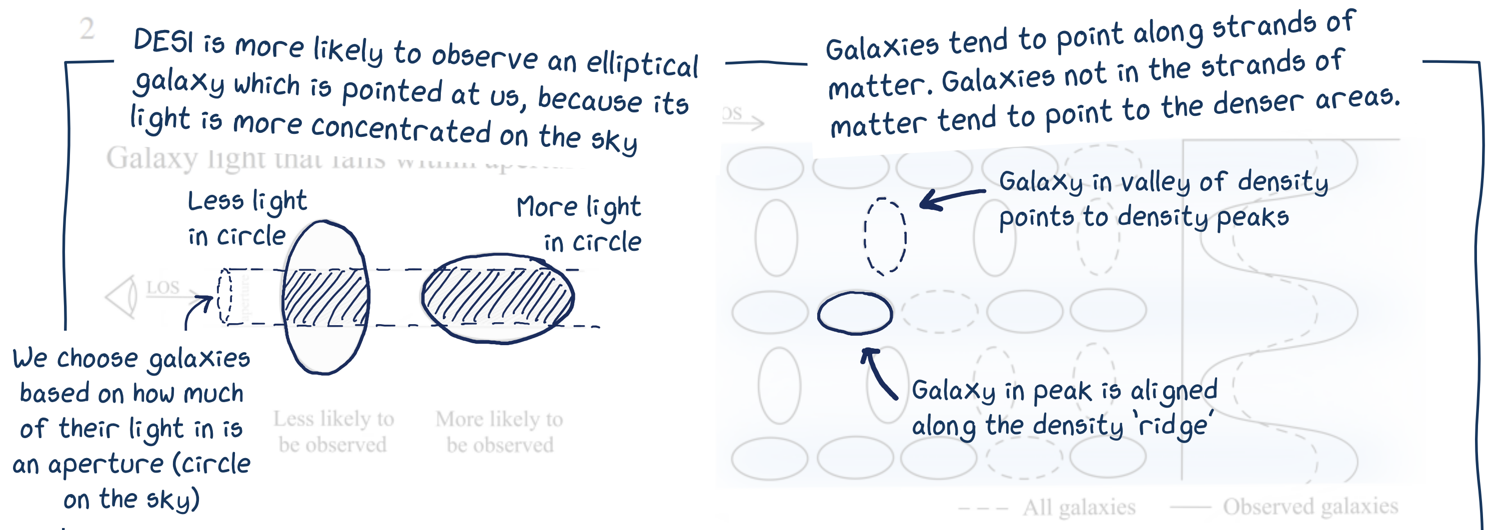

This figure explains the key idea of the paper and what we're trying to measure.

A bias in the orientations of galaxies we choose to observe + Galaxy orientation correlated with large structures of matter = A bias in how we measure the large structures of matter

One way we can measure how fast the structure grows is through an effect called RSD (Redshift Space Distortions). The bias we're studying creates a 'fake' RSD signal.

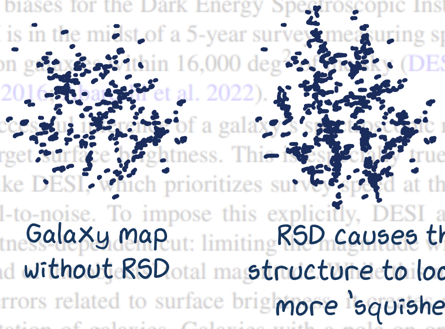

This is not a new idea, but DESI may be the first survey of its kind where it's actually an issue.

This is the first paper which has made a quantitative prediction of this "fake RSD". We hope to use it to correct DESI's measurements.

We also test these ideas by reproducing them with a simulated universe!

HOW WE GOT THE DATA

DESI is in the middle of its survey and hasn't measured the distances to all our galaxies yet. But we have pictures of them! Therefore we have the data we need: information about the shapes and colors of millions of galaxies.

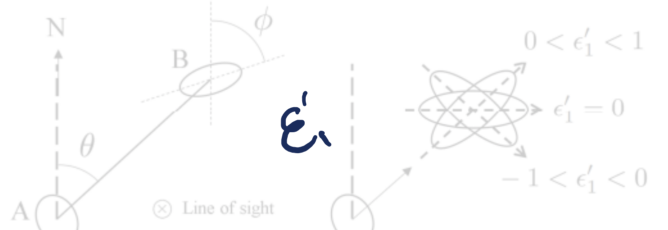

This figure explains how we quantify the shape of a galaxy. We can combine its orientation and how 'squished' it is into one number.

Figure 2. How angles are defined in our alignment metric. For a given pair of galaxies, ϵ'_1 is maximum when the ... (aligned) ... when it's perpendicular (anti-aligned). ϵ'_1 also scales with axis ratio; it approaches 0 as the shape of B becomes more circular.

detailed in 3.2. To conform with these weights, color outliers were removed by requiring $1 < r - W1 < 4.5$. Our final sample contained 17.5 million LRGs.

Generally, the redder a galaxy is, the further away it is. Since DESI has measured the distances to *some* galaxies already, we can calibrate a distance vs color relationship and use it to guess the distances to the galaxies which haven't yet been measured.

... spectroscopic redshifts from the DESI Survey Validation (SV) observations. SV is designed to represent the full survey and is used to assess ... which comprises of quality observations taken from 14 December 2020 through 10 June 2021. From this we selected 133,924 LRGs with colors $0.6 < r - z$ and $1.5 < r - W1 < 4.5$, and redshifts $0.001 < z < 1.4$.

3 INTRINSIC ALIGNMENT SIGNAL

3.1 Alignment Formalism

HOW WE MEASURE CORRELATIONS OF GALAXY SHAPES

The ... alignment of galaxies on the sky is quantified with ... (Figure 2). This measures the degree to which a galaxy is aligned with, and stretched along, a separation vector between it and another galaxy. Measuring this as a function of the separation vector's magnitude for many galaxy pairs is a way to quantify the alignment of LRGs to the underlying tidal field.

We treat every picture of a galaxy as an oval. This section describes how we use math to represent:

Here, 2D galaxy shapes are modeled as ellipses with a complex ellipticity

$$\epsilon = \frac{a-b}{a+b} \quad (1)$$

where a and b are the primary and secondary axis of the 2D ellipse, and ϕ is the orientation angle of the primary axis, measured East of North. We define the ellipticity of a galaxy B relative to another galaxy A using ... orientation angle, ϕ_B, and its position angle relative to A, θ_{BA}, also measured East of North.

1. The shape of each galaxy

$$\theta' = \phi_B - \theta_{BA} \quad (2)$$

2. How much that galaxy points towards other galaxies

This gives us a relative ellipticity, for which we measure the real component

$$\epsilon' = \frac{a_B - b_B}{a_B + b_B} \exp 2i\theta' \quad (3)$$

$$\epsilon'_1 = \mathrm{Re}(\epsilon') = |\epsilon'| \cos ... \quad (4)$$

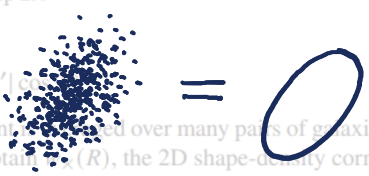

This measurement ... over many pairs of galaxies at varying separations to obtain $w_\times(R)$, the 2D shape-density correlation.

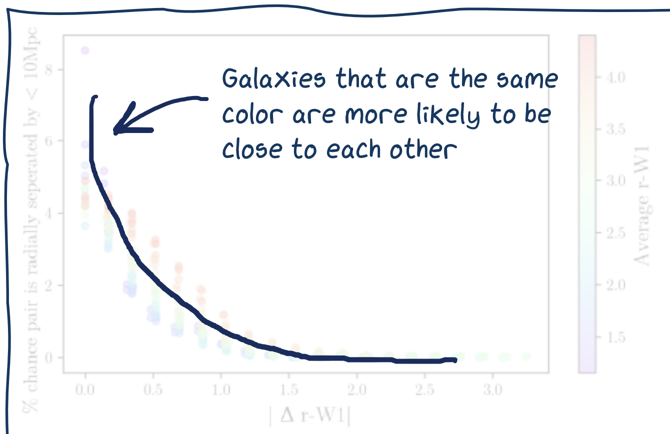

This figure is a visualization of how we connect the colors of two galaxies to the probability that they are the same distance away from Earth.

Figure 3. ... the alignment signal based on their color difference. This ... was created using a sub-sample of DESI galaxies with measured redshifts ... pairs which are more likely to be physically associated with each other.

3.2 Color Weighting

Just because two galaxies are in the same place in the sky, doesn't mean they're actually close to each other!

As our signal ... of its dilution is from pairs of galaxies with large radial separations. At the time of this paper, we do not have spectra for all of the imaged galaxies and ... color ... are more likely to be physically associated a higher weight in the alignment signal, we created a weighting scheme based off of their $r - W1$ colors.

Using the redshifts DESI has measured so far, described in Section 2.2, we separated galaxies into 20 bins of $r - W1$ color. We then calculated the fraction of galaxies which are radially separated by less than 10 Mpc for every combination of two colors, based on their redshift difference and assuming the Hubble flow. The resulting lookup matrix was then used as a weight when averaging the alignment signal from individual pairs (Figure 3).

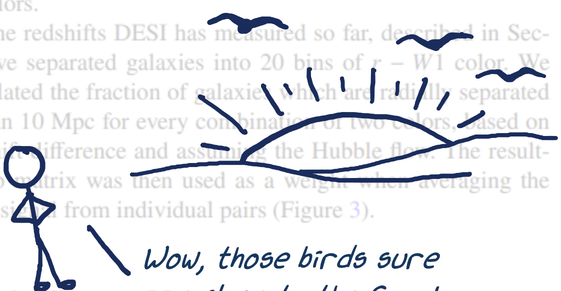

3.3 Intrinsic Alignment ...

The catalog was divided into 10 groups based declination and then each of those into 10 groups based on right ascension, resulting in 100 sky regions with an equal number of galaxies in each, 1.8 million. We measured the projected alignment of neighboring galaxies relative to each galaxy in each region. This was averaged over 20 bins of angular separation, resulting in 100 determinations of the IA signal. The average and standard error of these 100 measurements at each separation is our projected IA measurement, $w_\times(R)$[1].

Our final determination of $w_\times(R)$ for DESI LRGs is displayed in Figure 4. This signal broadly agrees with our measurement of projected IA in the Abacus Mock from Section 4, which did not include any ... orientations. The similarity between the alignment in LRGs and raw halo shapes is likely a coincidence due to two opposing effects: halo orientations are more aligned ... $w_\times$, but are rounder than LRGs, which dilutes $w_\times$. The LRG measurements of $w_\times$ in each angular bin are statistically independent of each other, as demonstrated by the ... between the 20 bins of radial separation (Figure 5).

Even though we don't know the distances to these galaxies (yet), we can use their colors and try to only make measurements of galaxies which are actually close to each other.

[1] code available here: github.com/cmlamman/ellipse_alignment

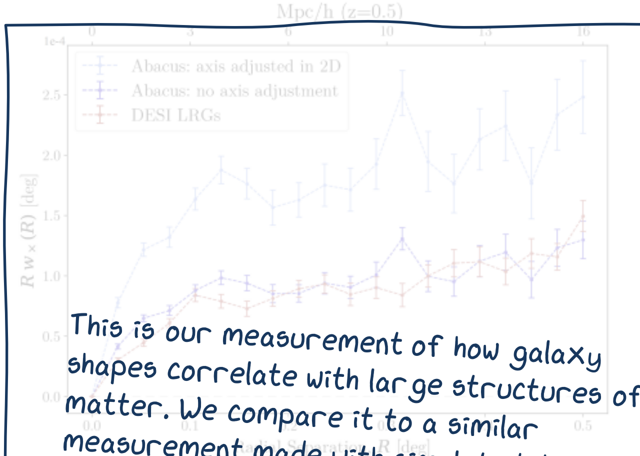

This is our measurement of how galaxy shapes correlate with large structures of matter. We compare it to a similar measurement made with simulated data, which is tricky because the simulation only simulates dark matter (see next section).

Figure 4. Our final measurement of the projected shape-density correlation of DESI LRGs, which includes weighting based on the color difference in galaxy pairs. This is compared to the same measurement with Abacus halos (dark blue). The light blue line shows the alignment of Abacus halos once the distribution of their projected shapes was adjusted to match the LRGs, but does not include galaxy-halo misalignments.

This is a fancy way of showing that the measurements we made above are not mixed up with each other

Figure 5. The reduced covariance matrix of $w_\times$ between bins of radial separation for our IA measurement; the identity matrix has been subtracted from this plot. This demonstrates that the measurements of $w_\times$ in each angular bin are statistically independent of each other.

3.4 Weak Lensing

DARN GRAVITY WARPS LIGHT

Besides intrinsic alignment, the main effect impacting the alignment signal is gravitational weak lensing. If the shape of a neighbor galaxy is measured relative to a foreground central galaxy, the neighbor's light can be gravitationally distorted by the central galaxy ... us.

Lensing: it makes JWST images pretty but it makes our data pretty messy.

Since we only measure the shape of one galaxy in each pair, weak lensing is only present when the measured galaxy is in front of the central one. Therefore a simple way to isolate the weak lensing and IA signals is to set restrictions on the radial separations of pairs. We compared the alignment for sets of pairs with various color restrictions (Figure 6). The signal from only measuring the shapes of galaxies relative ... measurement using color weighting. The signal from only measuring galaxy shapes

We're trying to measure the REAL shapes of galaxies. But gravity can act like a cosmic lens and distort light. This means that the actual shapes we see in a telescope are slightly warped.

In the first part of this section, we explain a neat way we can use galaxy colors to separate the signal caused by real galaxy shapes from the signal caused by lensed galaxy shapes.

relative to background galaxies is consistent with 0 above separations of a few Mpc/h and the signal from measuring galaxy shapes relative to foreground galaxies is, as expected, opposite in sign to the intrinsic signal.

To check whether the lensing signal is consistent with expectations, we consider the following approximate model. The net effect of weak lensing ... tangential shear on the sky:

$$\gamma_t = \frac{\bar{\Sigma}(<r) - \Sigma(r)}{\Sigma_{\rm crit}} \tag{5}$$

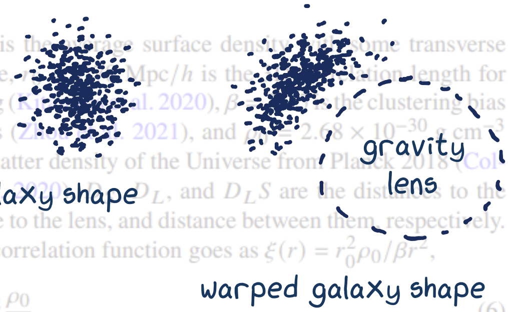

where $\bar{\Sigma}(<r)$ is the average surface density within some transverse distance r. Here, r_0 = ... Mpc/h is the correlation length for DESI clustering (Kitanidis et al. 2020), β ... the clustering bias for DESI LRGs (Zhou et al. 2021), and $\rho_0 = 2.68 \times 10^{-30}$ g cm^{-3} is the critical matter density of the Universe from Planck 2018 (Collaboration et al. 2020). D_S, D_L, and D_LS are the distances to the source, distance to the lens, and distance between them, respectively. Assuming the correlation function goes as $\xi(r) = r_0^2\rho_0/\beta r^2$,

$$\bar{\Sigma}(<r) = \frac{2\pi}{r} r_0^2 \frac{\rho_0}{\beta} \tag{6}$$

$\Sigma(r)$ is the average surface density at r

$$\Sigma(r) = \frac{r_0^2}{r}\pi\frac{\rho_0}{\beta} \tag{7}$$

and $\Sigma_{\rm crit}$ is the critical mean density, above which the light of a source is split into multiple images.

$$\Sigma_{crit} = \frac{c^2}{4\pi G}\frac{D_S}{(1+z_l)D_L D_{LS}} \approx \frac{c^2 D_S}{4\pi G D_L D_{LS}} \tag{8}$$

In the second part of this section, we lay out the theory for how we can predict what effect lensing will have on our signal.

To connect this to our alignment formalism described in Section 3.1, the tangential shear ...

$$\gamma_t = \frac{a-b}{a+b}e^{2i\phi} \tag{9}$$

where ϕ is the azimuthal angle of the source galaxy's primary axis with respect to the lens. This ...

$$\bar{\epsilon}_1{}' = \frac{\bar{\gamma}_t}{-2} \tag{10}$$

To measure this in our sample, we used photometric redshifts to estimate $D_S/D_L D_{LS}$ for every pair of galaxies, and average the result. We used a simple, linear fit of our DESI spectroscopic sample for redshifts:

$$z = 0.25(r - W1) - 0.02 \tag{11}$$

The resulting lensing estimation is shown in Figure 6 and agrees well with the IA measurement made when limiting to pairs we expect are only affected by lensing. This final IA signal is likely still diluted by weak lensing. However we did not develop a more sophisticated adjustment for lensing, as DESI's first year of spectra will allow us to sufficiently isolate physically-associated pairs.

4 IA WITH ABACUS MOCK CATALOG

To contextualize the measured IA signal, we built a mock catalog from the AbacusSummit CompaSO halo catalog (Hadzhiyska et al. 2021). AbacusSummit is a suite of large, high-accuracy, high-resolution cosmological simulations made with the Abacus N-body code (Garrison et al. 2021). We used halos from a box with comoving 2000 h^{-1}Mpc sides, simulated at $z = 0.725$.

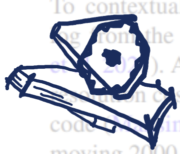

Turn page to see what we did with a dark matter simulation!

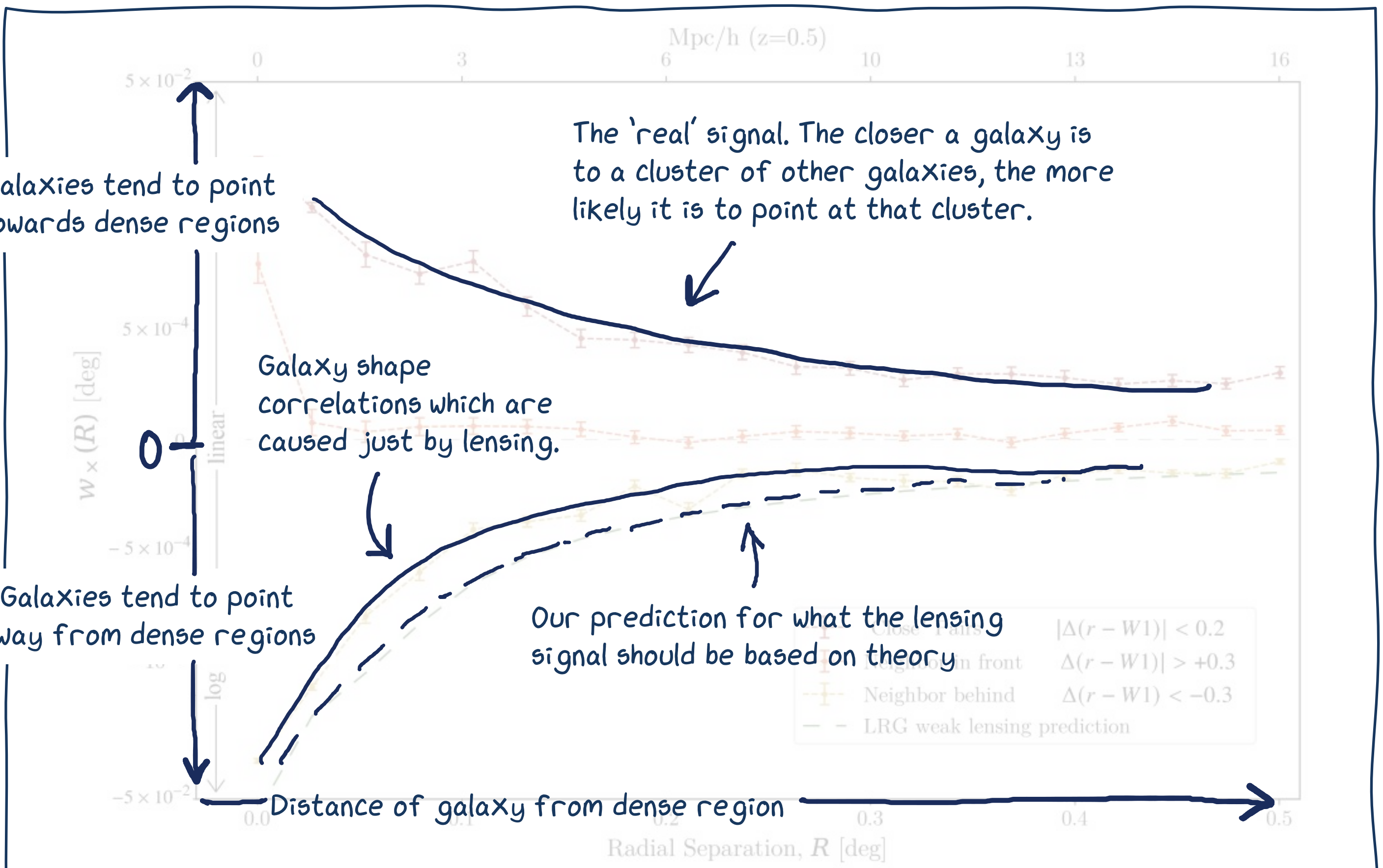

Figure 6. The shape-density correlation of DESI LRGs, resulting from measuring the shape of one "neighbor" galaxy relative to the separation vector between it and ... galaxies in order to explore the effects of weak lensing on the IA signal. The dark red line is the resulting signal when only measuring galaxy pairs which have a very s... a large difference in ... color, to emulate pairs which have no physical association. For the measurement shown in orange, we used pairs in which the neighbor galaxy ... we only measured the shape of galaxies relative to ones behind it, so their shapes were broadly unaffected by weak lensing. The converse was applied for the signal shown in yellow; here we only measured the shape of a galaxy if it was much redder than its counterpart. This means that the measured shape correlation is dominated by weak lensing.

The measurements described in the last section – how we separate the signal of real galaxy shapes from the signal of shapes which have been distorted by gravitational lensing.

COMPARING TO SIMULATED DATA

This section is all about how we reproduced our measurements of real galaxies with a simulation. This is tricky because the simulation only includes dark matter, so we're comparing big blobs of invisible matter to tiny bits of visible matter.

We mapped the halos' comoving positions to redshift and sky coordinates by placing an observer 1700 h^{-1}Mpc away from the center of the box along the x-axis. To have an even sky distribution and consistent redshift range across the sky, we set boundaries of $\pm 12°$ in right ascension and declination, with a redshift range of ...

We then selected the largest halos to match both the LRG density of our DESI sample within this redshift range, ... and the redshift distribution from DESI spectra. Our final mock catalog contains 766,341 halos.

To imitate the DESI Legacy Imaging Survey colors, we used a catalog of DESI LRG spectroscopic redshifts, sorted by redshift. For each halo, we identified the LRG with the closest redshift. We then smoothed our selection ... Gaussian of indices centered at the index of closest redshift and with a width of 300. TAfter taking the $r - W1$ color from the LRG with the resulting index, we again ... at that color with a width of $\sigma = 0.03$. These smoothing parameters sufficiently reproduced the observed data spread, and variations of them do not significantly affect the measured alignment signal.

The Abacus ... halo shapes are modeled as triaxial ellipsoids. A common method for finding the projected axis ratios of ellipsoids can be found in Binney (1985). For measuring the alignment of galaxy shapes, we additionally need the orientation angle of the projected shape. Therefore, we adapted the method derived in Gendzwill & Stauffer (1981) to project triaxial ellipsoids onto the celestial sphere. Our process for obtaining the axis ratio and orientation of an ellipsoid ... A.

... of the projected halos to the LRG axis ratio distribution. We adjust each axis ratio, $b/a = d$, with the empirical function:

$$d' = 1 + 1.1(d - 1) - 2.035(d - 1)^2 + 1.76(d - 1)^3 \quad (12)$$

This function correctly reproduces the number of observed axis ratios which fall in 100 bins between 0 and 1. ...

Using the same color-weighting scheme as described in Section ... of our resulting mock catalog. The result can be seen in Figure 4. The higher amplitude is likely due to the simulation not including the effects of weak lensing and the higher degree of alignment in halos compared to galaxies. Tenneti et al. (2014) estimates large, central galaxies at DESI redshifts to be misaligned with their host halo by an average

The dark matter blobs, or "halos" are better representatives of what the large cosmic structure is actually like. Galaxy shapes are more random. Dark matter halos are also much rounder than galaxies, so we need to account for this too.

of around 10-20°. This propagates to a $w_\times$ signal that is 75-94% of the same signal without misalignments.

USING MATH TO CONNECT ALL THE PARTS OF THIS PAPER

5 MODELING ALIGNMENT - ξ_2 CORRELATION

5.1 Linear Tidal Model

We adopt a linear tidal model to connect IA and DESI's shape selection bias with the quadrupole of the correlation function, ξ_2. This approximation assumes that the projected shapes of galaxies are linearly related to the projected density distribution and holds for LRGs above projected separations of 10 h^{-1}Mpc (Catelan & Porciani 2001; Hirata & Seljak 2004; Singh et al. 2015; ...).

At this point, we've measured how the shapes of galaxies correlate with the large, underlying structure of matter. But how exactly is this measurement connected with the galaxy statistics that DESI cares about?

We define $\nabla^2\phi = \rho$, where ρ is the fractional over density. The tidal tensor is then the traceless combination $T_{ij} = \partial_i\partial_j\phi - (1/3)\delta^K_{ij}\nabla^2\phi$, where δ^K is the Kronecker delta.

We model the mean 3D ellipticity of a triaxial galaxy as τT_{ij}, where the axis lengths behave as $I+\tau T$. For this derivation, we assume that 2D projections of such galaxies behave as the 2D projection of these lengths. The mean eccentricity tensor must also be traceless, so for a projection with $\alpha, \beta = \{x, y\}$, the projected ellipticity is given as $\epsilon_{\alpha\beta} = \tau(T_{\alpha\beta} + T_{zz})$, where we used $T_{xx} + T_{yy} = -T_{zz}$.

Using Fourier-space conventions and the matter power spectrum $\left\langle\tilde{\rho}(\vec{q})\tilde{\rho}^*(\vec{k})\right\rangle = (2\pi)^3 P(\vec{k})\delta^D(\vec{q}-\vec{k})$, we have the tidal tensor model:

$$T_{ij}(\vec{r}) = \left(\partial_i\partial_j - \frac{\delta^K_{ij}}{3}\nabla^2\right)\int\frac{d^3k}{(2\pi)^3}\tilde{\phi}(\vec{k})e^{i\vec{k}\cdot\vec{r}}$$

Using a basic* model, we get this relation:

$$= \int\frac{d^3k}{(2\pi)^3}\left(\frac{k_ik_j - \delta^K_{ij}k^2/3}{k^2}\right)\tilde{\rho}(\vec{k})e^{i\vec{k}\cdot\vec{r}} \quad (13)$$

5.2 Shape-Density Correlation

To consider the correlation of galaxy ellipticity with surface density, we begin with the expression for the projected fractional overdensity for a survey of functional depth L and uniform mean density $\bar{\rho}$:

$$\boxed{\text{The "fake" RSD signal}} \propto \boxed{\text{How much the shapes of galaxies correlate with large-scale structure}} \times \boxed{\text{How much galaxies in the survey tend to be pointed towards Earth}}$$

$$\Sigma(R) = \frac{1}{L}\int dz\,\rho(R,z) \quad (14)$$

where $\hat{z}$ is along the LOS and $\vec{R}$ is projected separation. L is a measure of how far along the LOS we average when measuring $\epsilon_{\rm LRG}$. As our survey is not homogeneous, we generalize L to an expression of $w(i,j)$. Using the weights ... galaxy pairs, we sum over all combinations of color bins $B1$, $B2$, and galaxy pairs j, k. This is averaged per bin and multiplied by the depth of that bin B_d.

i.e.– the more galaxy correlation we see, and the more bias there is in galaxy shapes, the bigger problem we have.

$$L = B_{\rm d}\frac{\Sigma_{B1}\Sigma_{B2}\Sigma_{\rm i}\Sigma_{\rm j}w(i,j)}{\Sigma_{B1}\Sigma_{\rm i}\Sigma_{\rm i}w(i,j)} \quad (15)$$

The projected ellipticity is $\hat{R}_\alpha\epsilon_{\alpha\beta}\hat{R}_\beta$. For the average, we can just consider the $\hat{R} = \hat{x}$ direction. The shape-density correlation projected onto the plane of the sky is then given as

$$w_\times(R) = \langle\epsilon_{xx}\Sigma(R\hat{x})\rangle = -\frac{\tau}{L}\left\langle T_{yy}\int dz\,\rho(R\hat{x},z)\right\rangle \quad (16)$$

We compute and simplify this expression (Appendix B1) to

$$w_\times(R) = \frac{\tau}{3L}R^2\frac{d}{dR}\left[\frac{1}{R^2}\Psi(R)\right] \quad (17)$$

where we introduce

$$\Psi(R) = -\frac{d\Phi}{dR} = \int\frac{K\,dK}{2\pi}\frac{P(K)}{K}J_1(KR) \quad (18)$$

K is 2D Fourier Space, P is the power spectrum, and J_1 is the first Bessel function.

τ can be inferred from our measurement of the shape-density correlation, $\langle\epsilon_{xx}\Sigma(R\hat{x})\rangle$, showing that the LOS shape and ξ_2 are correlated. We estimate τ as

$$\tau_{\rm obs} = \frac{3Lw_\times}{R^2\frac{d}{dR}\left[\frac{1}{R^2}\Psi\right]}, \quad (19)$$

with our IA measurement, $w_\times$, and averaging over angular scales R.

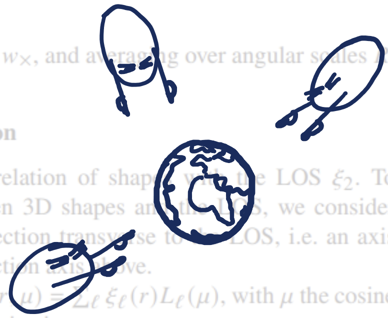

5.3 Shape - ξ_2 Correlation

Next, we turn to the correlation of shapes with the LOS ξ_2. To obtain the relation between 3D shapes and the LOS, we consider shapes viewed from a direction transverse to the LOS, i.e. an axis perpendicular to the projection axis above.

Since we define ξ_2 as $\xi(r,\mu) = \sum_\ell \xi_\ell(r)L_\ell(\mu)$, with μ the cosine of the angle to the LOS, ξ_2 is given as

$$Q(r) = 5\int\frac{d^2\hat{r}}{4\pi}\rho(\vec{r})L_2(\mu) \quad (20)$$

No, this doesn't mean Earth is special. This is not a real property of the Universe. It's caused by how DESI (located on Earth) chooses its targets, and is explained more later.

where $\int d^2\hat{r}$ indicates the 2D integral over the unit vector $\hat{r}$.

To express the transversely viewed shape, we take the average of ϵ_{xz} and ϵ_{yz}, each after the correction to a traceless quantity. For the x–z projection, we have $\epsilon_{zz} = \tau(T_{zz} + T_{yy})$, where the relevant quantity is ϵ_{zz}. Averaging with the y–z projection, we have a transverse averaged eccentricity

$$\epsilon_{zz} = \tau\left(T_{zz} + \frac{T_{xx}+T_{yy}}{2}\right) = \frac{\tau}{2}T_{zz} \quad (21)$$

Considering projections along $\hat{x} \pm \hat{y}$ also yield $T_{zz}/2$ as the only $m = 0$ support.

The details of computing and simplifying ... can be found in Appendix B2, which result in

$$\langle\epsilon_{zz}Q(r)\rangle = -\frac{\tau}{3}\int\frac{q^2dq}{2\pi^2}P(q)j_2(qr). \quad (22)$$

This expression is averaged over radial bins of the correlation function, resulting in averages of $j_2(qr)$.

5.4 Bias ...

We expect the mean shape to be elongated along the LOS due to DESI's target selection, i.e. a non-zero mean ϵ_{zz} (Section 6). We call this LOS polarization $\epsilon_{\rm LRG}$.

Assuming ϵ_{zz} and the quadrupole signature Q are Gaussian distributed, correlated, random variables, a non-zero $\langle\epsilon_{zz}\rangle$ will result in a non-zero mean $Q(r)$ as

$$\langle Q\rangle = \langle\epsilon_{zz}\rangle\frac{\langle\epsilon_{zz}Q\rangle}{\langle\epsilon_{zz}^2\rangle}. \quad (23)$$

where the expectation values come from summing over each galaxy. From our tidal model,

$$\left\langle\epsilon_{zz}^2\right\rangle = \frac{\tau^2}{4}\left\langle T_{zz}^2\right\rangle \quad (24)$$

$$= \frac{\tau^2}{45}\int\frac{q^2dq}{2\pi^2}P(q). \quad (25)$$

* Do NOT let this word fool you. It was the simplest model we could use, but oohhh man was it a pain to figure out.

This is the variance in the density field σ^2, hence $\langle \epsilon_{zz}^2 \rangle = \tau^2\sigma^2/45$.

Combining the above results, we obtain an expression for the quadrupole signature arising from GI alignment and a shape-dependent selection bias:

$$\xi_{\rm GI} = \langle Q(r) \rangle = \epsilon_{\rm LRG} \frac{\tau}{3\langle \epsilon_{zz}^2 \rangle} \int \frac{q^2 dq}{2\pi^2} P(q) j_2(qr) \quad (26)$$

GALAXIES ARE POINTING AT EARTH???

6 MODELING DESI'S SELECTION EFFECTS

In Section 3 we measured how the shapes of galaxies projected onto the sky are aligned with the density field. To infer how this affects RSD measurements, we need to estimate the extent of DESI's orie[illegible] galaxies have a higher surface brightness and are more likely to pass selection, we expe[illegible] polarization ϵ_{LR}[illegible]) relative to the LOS.

...well, there's a VERY small tendency for galaxies to be pointing at us. And it's only in the sample of galaxies that DESI has chosen to observe.

W[illegible] LRGs which is similar to the sample described in Section 2.1, except without the fiber magnitude cut. We assign each parent LRG a 3D galaxy light profile, then simulate images of each profile from all viewing angles, without any extinction from internal dust. The polarization is the average $\epsilon_{1,\rm LOS}$ of all 3D profiles which pass selection.

6.1 Parent Sample

We estimate polarization using a subsection of DESI LRGs in an area of the sky with the best-resolved shapes, with right ascension and declina[illegible] is in the South Galactic Cap (SGC) and part of the Legacy Imaging Survey's DES region. This parent sample of 41120 objects has the same cr[illegible] z-magnitude cut of $z'_{\rm fiber} < 21.61$ for the SGC. The fiber magnitude comes [illegible] shape model with a standardized PSF. This somewhat isolates the fiber magnitude from seeing variations, so we can safely use shapes from an area with the best seeing without impacting the distribution of underlying shapes. As in Section 2, we also use shape parameters from the best-fit, non-circular, mode[illegible] 0.9[illegible] of this sample have the same fiber z-magnitude as total z-magnitude. This indicates that these objects are either stars or unresolved galaxies. We ignored these objects for our analysis, but a more thorough simulation would involve simulating galaxies through the TRACTOR pipeline, as is done with [illegible] 2020).

This is the effect shown in the first part of Figure 1. Galaxies which 'point' at Earth, i.e. their longest axis is oriented towards us, are more likely to be chosen. This is because their light is more concentrated on the sky, and more light in a smaller area = better chance that we can get good measurements of it.

We estimate this by creating LOTS and LOTS of fake galaxies (like, millions), taking care to give them realistic 3D shapes and realistic light profiles.

6.2 Light Profiles

Our light profile for each galaxy begin as a realization of 100,000 points. This representation allows us to rapidly apply the triaxial axis lengths, rotations, and projections, as well as to apply a 2D Gaussian PSF (by de[illegible]) and the eventual [illegible].

The points [illegible] given galaxy are distributed in 3D based on its best-fit shape [illegible] from the parent catalog. DESI's TRACTOR pipeline represents projected galaxy shapes as a mixture of Gaussians (Hogg & Lang 2013). To de-project these [illegible], we take advantage of the fact that a 3D Gaussian proj[illegible] Gaussian. Therefore the 2D Gaussian mixture fits allow us to [illegible] construct a 3D model. This was done for all parent LRGs with a best-fit profile of Vau[illegible], exponential, and round-exponential LRGs. Relatively

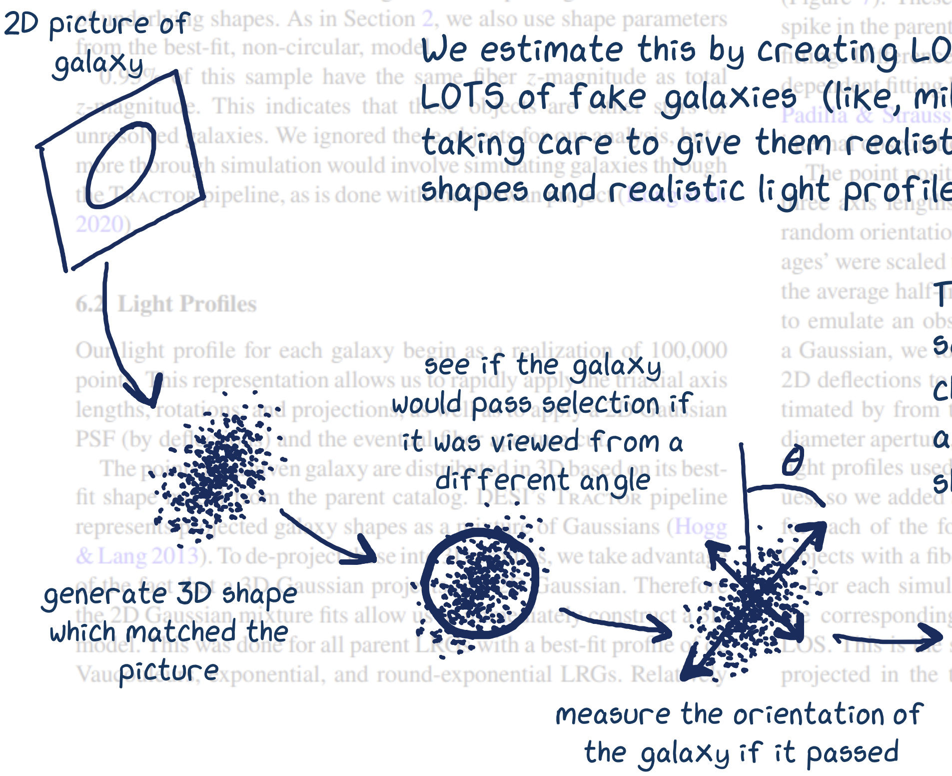

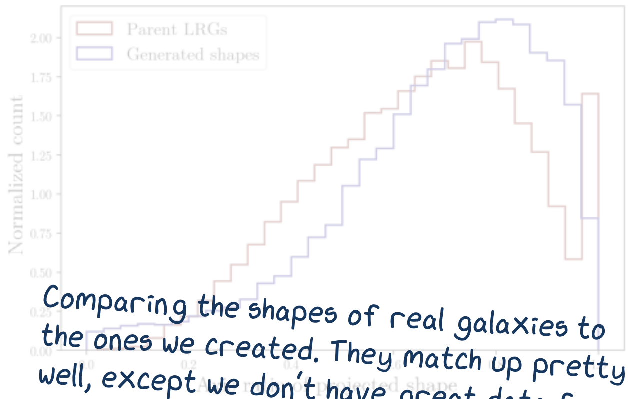

Figure 7. A comparison of the [illegible] sample and the projected [illegible] of triaxial shapes. These are the triaxial shapes used in our polarization estimate. The spike at $b/a = 1$ in the parent sample is artificial, likely due to poor shape fitting.

few LRGs were fit best with a Sersic profile. These tend to be bright enough that they are not near the aperture magnitude cut and therefore less affected by this biased selection; for simplicity we modeled these with a Hernquist profile (Hernquist 1990).

6.3 Polarization Estimate

For each object in the parent sample, we assign a triaxial shape based on its projected shape. These were randomly drawn from the expected distribution of triaxial shapes for bright ($M_r > -19$), medium ($2 < r_{gal} < 7h^{-1}$ kpc) ellipticals in imaging from the Sloan Digital Sky Survey (Padilla & Strauss 2008). 41120 3D shapes were projected along a random viewing angle and ranked by the axis ratio of the resulting ellipse. The LRG parent sample was also sorted by axis ratio, and matched with the triaxial shape corresponding to the projected shape of the same rank.

To test these triaxial shapes, we viewed them each from a different angle and compared the projected axis ratios to our parent sample (Figure 7). These distributions are not identical; note the artificial spike in the parent sample at $b/a = 1$ which is likely from poor shape fitting. [illegible] distributions could also be due to shape-dependent fitting biases in TRACTOR, or imperfect distributions from Padilla & Strauss (2008), including shape evolution from z = 0 or [illegible].

The point positions from Section 6.2 were scaled by the assigned three axis lengths for each galaxy. They were then rotated to 100 random orientations and projected along one axis. The resulting 'images' were scaled using the ratio of the observed half-light radius and the average half-light radius of all model orientations. We next [illegible] to emulate an observation in 1″ seeing. Instead of convolving with a Gaussian, we took the quicker approach of adding pre-computed 2D deflections to the projected points. The fiber magnitude was estimated by from the fraction of points which fell within an 1.″5 - diameter aperture [illegible] light profiles used did not perfectly replicate the observed $z_{\rm fiber}$ values, so we added a calibration factor to the N-body fiber magnitude for each of the four light profiles to match the true $z_{\rm fiber}$ median. Objects with a fiber magnitude less than 21.61 passed selection.

Then we push them through the same process that DESI uses to choose targets and measure the average orientation of the 3D shapes which pass the cut.

For each simulated image which passed selection, we measured the corresponding 3D profile's complex ellipticity relative to the LOS. This is the same convention as Equation 4, except shapes are projected in the transverse direction. The average of these is our

Some pretty visualizations of the orientation bias in DESI's galaxies.

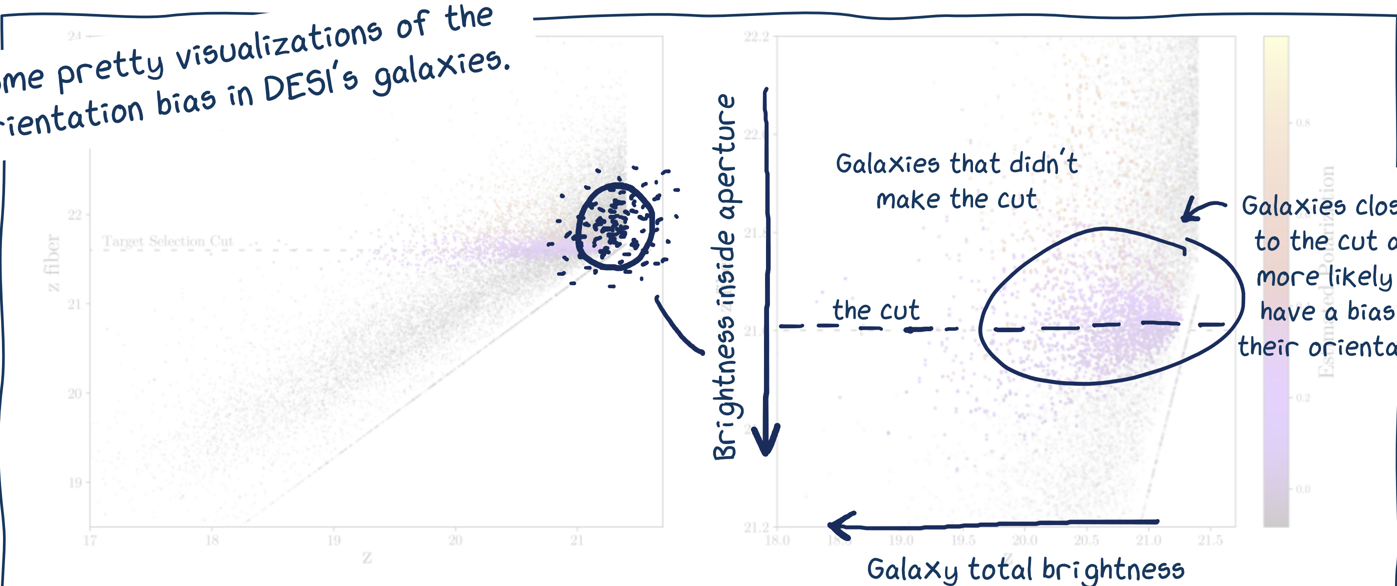

Figure 8. Results from our N-body reproduction of DESI's target selection. There are two main flux cuts on the LRGs: a sliding $r - W1$ vs $W1$ cut which dominates at bluer colors, and the z_{fiber} cut which dominates at redder colors. The full parent sample is shown on the left and a closer look near the fiber magnitude cut on the right. Each galaxy was assigned a triaxial shape, which was rotated to 100 random orientations. Its polarization is the average ellipticity relative to the light of sight of the objects which passed an aperture-magnitude cut. For target selection, we find that the orientation of shapes matters only for objects very close to the fiber magnitude cut, and is more likely to matter for more elliptical galaxies.

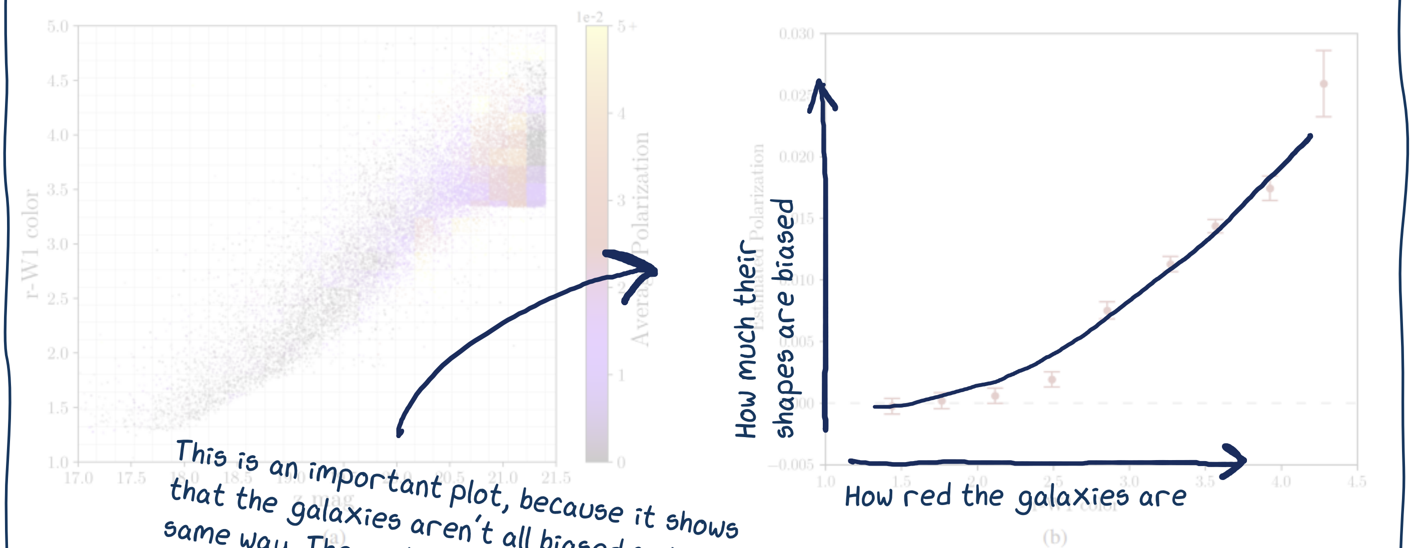

Figure 9. Properties of fake targets from our simulated images. a: the z mag and color taken from a parent sample of LRGs. Each square is colored by the average polarization of that bin. We attribute the drop in polarization near the highest z mag to a selection effect: in order for these targets to pass selection they must have a fiber magnitude very close to their total magnitude, resulting in more compact shapes and a dampened polarization. b: the polarization of selected targets binned by color. We expect this trend, since fainter galaxies tend to fall closer to the fiber-magnitude cut (Figure 8). A higher polarization for redder colors could lead to an increased ξ_2 bias at higher redshifts and mimic structure growth.

polarization ϵ_{LRG}. 54.2% of our simulated galaxy images passed the fiber magnitude cut, similar to the actual value of 52.9%. The polarization for these galaxies is 0.0087 ± 0.0002. By determining the selection of a set of orientations for each galaxy shape, we can also estimate which galaxies in the original sample may have an orientation-dependent selection (Figure 8). To see what polarization DESI can expect in its targets, we've plotted the average polarization in bins of z mag and $r - W1$ color (Figure 9a).

We also find that the redder LRGs may be more affected by orientation. This translates to a correlation between redshift and polarization, which could affect studies of structure evolution (Figure 9b).

Just how big is this orientation bias?

We call the tendency for galaxies to be pointing at Earth "ε_{zz}".

If galaxies had random orientations → $\varepsilon_{zz} = 0$

If galaxies were sticks that all pointed at Earth → $\varepsilon_{zz} = 1$

What we measure → $\boxed{\varepsilon_{zz} = 0.009}$

7 ESTIMATE OF ξ_2 BIAS

At this point, we have measured all the necessary components to estimate the ξ_2 signature arising from IA and DESI's selection bias.

ϵ_{LRG}, the polarization of galaxy shapes along the LOS, is measured in Section 6. $\langle \epsilon_{zz}^2 \rangle$ is the variance of the real part of the complex ellipticities which describe the shapes of DESI's LRGs and is 0.031.

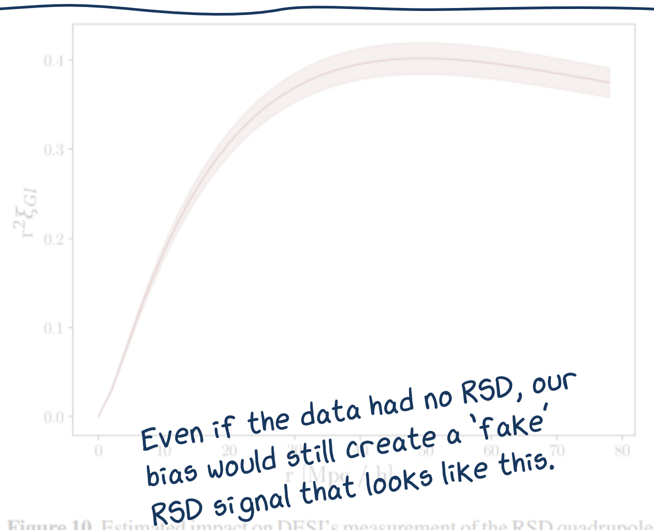

Figure 10. Estimated impact on DESI's measurement of the RSD quadrupole. This about corresponds to a 0.5% error for separations around 40-80 h^{-1}Mpc based on SDSS-III BOSS measurements (Anderson et al. 2014). The precision of our estimate is shown in the shaded region as the standard error.

We used the power spectrum, $P(K)$ from AbacusSummit (Maksimova et al. 2021).

PUTTING IT ALL TOGETHER

τ is a function of effective depth L, or how far along the line of sight we average when measuring ϵ_{LRG}. This was estimated using the color weighting scheme from Section 3.2 to be $L = 865h^{-1}$Mpc

After shoving all our measurements through the equations in the "math" section, we have a result!

projected separation, we estimate $\tau_{obs} = -0.174$.

together, we determine $r^2\xi_{GI}$ to be $3.5h^{-1}$Mpc around 10-80 h^{-1}Mpc. The full separation dependence is shown in Figure 10. SDSS-III measures

We predict that DESI's measurements of RSD will be lowered by about 0.5%

This puts our estimate of the fractional error on ξ_2 around 0.5% at

8 ξ_2 BIAS WITH ABACUS

REPRODUCING EVERYTHING WITH THE SIMULATION

on produces a false ξ_2 signature and test our linear tidal model connecting the GI and RSD signals, we model the problem using Abacus Summit simulations.

As in Section 4, we started with a 2000 h^{-1}Mpc box of large halos and mapped their positions to redshift, right ascention, and declination. Sky cuts were applied to ensure a uniform sky distribution at each redshift.

But how can we be sure that our equations are spitting out the right answer? One way to do a reality check is with the simulated universe from before.

To see how an aperture selection impacts the ξ_2 measurement, we created two samples: one without any selection, and one only with halos containing more than than 48,000 points within the aperture, which corresponds to 50% of the halos. We measured $\xi_2(r)$ for both in real space space and in redshift space, using the halo's original velocities.

We're so close to figuring out the question...

$\xi_2(r)$ was determined using the Landy-Szalay Estimator (Landy

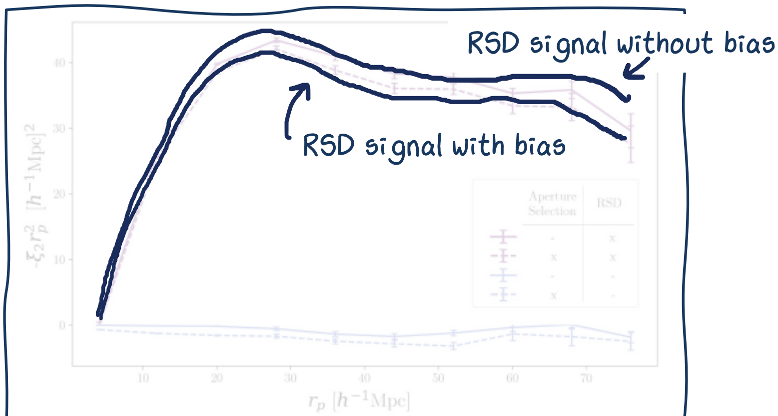

Figure 11. Results from reproducing our measurements with a simulation

with and without an aperture-based selection. The top lines include Redshift-Space Distortions. The aperture-based selection creates an artificial, non-zero RSD signature, which acts in opposition to ξ_2 on large scales.

& Szalay 1993) and averaged over 10 sets of randoms, generated with random right ascension and declinations for each redshift. This

We use the simulation to create fake data, then measure the RSD signal before and after we apply the target selection which biases orientations.

cut was $\epsilon_{LRG} = 7.6 \pm 0.1 \times 10^{-3}$. The resulting prediction is compared to the model in Figure 12.

We expect the bulk of the disagreement between these two simple models to be due to the linear approximation, which does not hold at lower separations, and simplifications in the demonstration mock.

We also compare this to what our equations predict would be the RSD bias for this fake data (result in plot on next page).

9 CONCLUSION

CONCLUSION

study is to determine the approximate impact on DESI's RSD measurements due to an orientation bias in LRGs. We have demonstrated that the effect is significant for DESI and estimate

Soooooo all of this work for a bias that's only..... 0.5%.

To reduce the effects of intrinsic alignment for DESI, simple yet severe choices involve only measuring ξ_2 in galaxy subsamples, per-

What's the big deal??

could be used for calibration.

As the DESI survey progresses and the precision in ξ_2 increases, there are several opportunities to improve our bias estimate. Our

It sort of is a big deal. The reason DESI is surveying so many galaxies is so we can get verrry precise measurements of the Universe's structure.

polarization. We match the expected distribution of projected shapes in a region of the sky with the best shape fits, but 5.6% of galaxies

continued

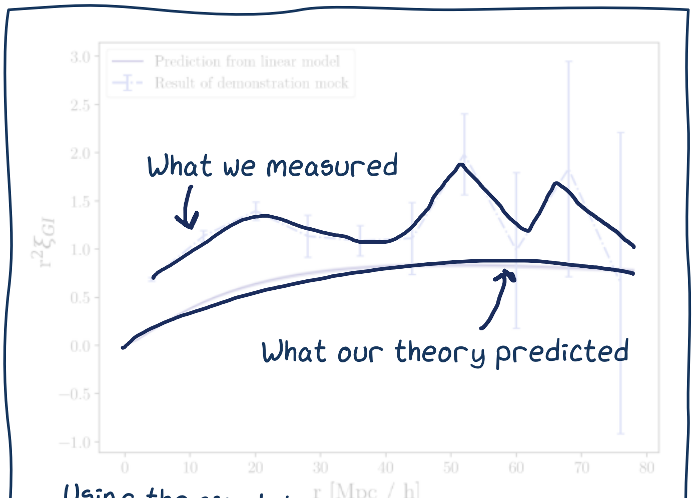

Using the simulation to check our theory. Although these lines don't *look* very close, they're actually good enough for this basic reality check.

Figure 12. ... tion. ... the difference between the measurements of ξ_r in Figure 11 without RSD. The model gets close, but appears to be about 40% lower.

in this subsample are fit as circles, creating an artificial spike at ... accurate shapes, ie from the Dark Energy Survey (Gatti et al. 2021), ...

Believe it or not, 0.5% could make the difference between competing models of dark energy. They call it "precision cosmology" for a reason!

Although partially mitigated by color weighting, the IA signal in this work is reduced by weak lensing and diluted by the inclusion of ... This will be drastically improved with DESI's first year of data, which contains 2.5 million quality LRG spectra. The LOS distance we average over due to uncertainty in radial distances, $L = 865h^{-1}$Mpc, will decrease by a factor of at least 20 with redshifts. Advancing our ability to measure IA for only pairs of galaxies which are physically associated will be the strongest improvement to the false ξ_2 estimate.

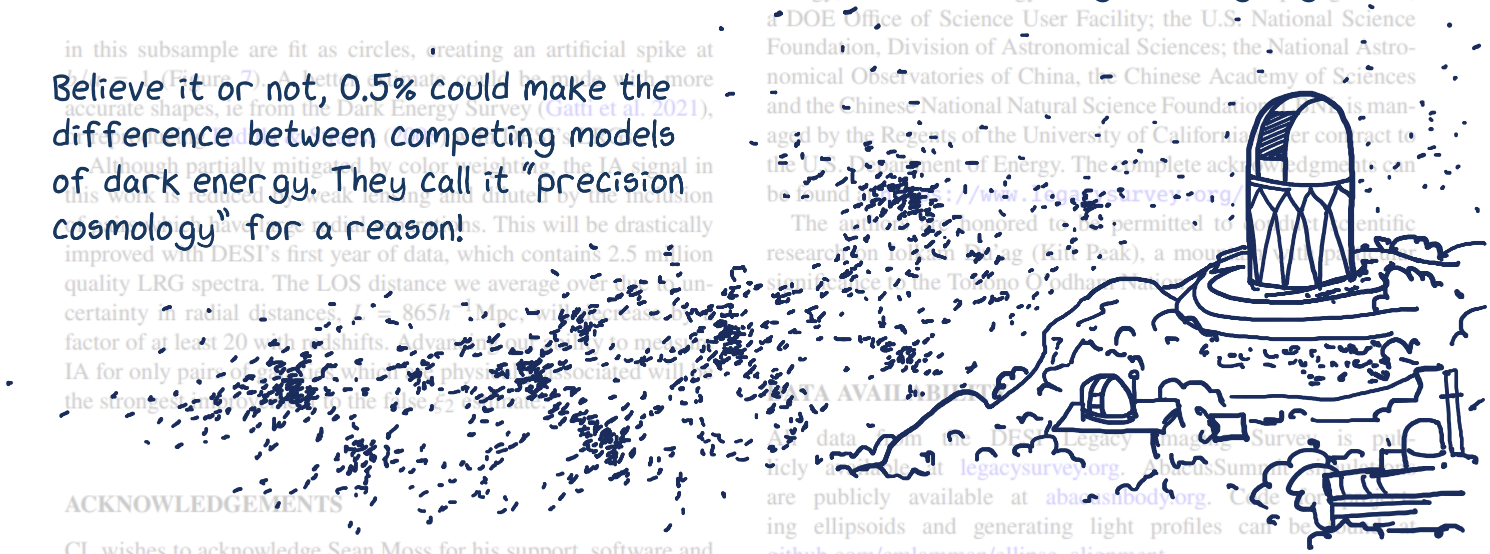

ACKNOWLEDGEMENTS

CL wishes to acknowledge Sean Moss for his support, software and otherwise, and Tanveer Karim for many helpful conversations. The authors also thank Eric Jullo, Eusebio Sanchez, Robert Kehoe, and Zachary Slepian for their input through the collaboration review process.

This material is based upon work supported by the National Science Foundation Graduate Research Fellowship under Grant No. DGE1745303, the U.S. Department of Energy under grant DE-SC0013718, and NASA under ROSES grant 12-EUCLID12-0004. DJE is further supported by the Simons Foundation.

WE DIDN'T DO IT ALONE

It takes many individuals, institutions, and funding agencies to make a project like DESI happen!

This research is also supported by the Director, Office of Science, Office of High Energy Physics of the U.S. Department of Energy under Contract No. DE–AC02–05CH11231, and by the National Energy Research Scientific Computing Center, a DOE Office of Science User Facility under the same contract; additional support for DESI is provided by the U.S. National Science Foundation, Division of Astronomical Sciences under Contract No. AST-0950945 to the NSF's National Optical-Infrared Astronomy Research Laboratory; the Science and Technologies Facilities Council of the United Kingdom; the Gordon and Betty Moore Foundation; the Heising-Simons Foundation; the French Alternative Energies and Atomic Energy Commission (CEA); the National Council of Science and Technology of Mexico (CONACYT); the Ministry of Science and Innovation of Spain (MICINN), and by the DESI Member Institutions: https://www.desi.lbl.gov/collaborating-institutions.

In the conclusion, we're also very careful to explain assumptions we made. The point of this paper is mainly to get an estimate of how big this effect will be for DESI.

The DESI Legacy Imaging Surveys consist of three individual and complementary projects: the Dark Energy Camera Legacy Survey (DECaLS), the Beijing-Arizona Sky Survey (BASS), and the Mayall z-band Legacy Survey (MzLS). DECaLS, BASS and MzLS together include data obtained, respectively, at the Blanco telescope, Cerro Tololo Inter-American Observatory, NSF's NOIRLab; the Bok telescope, Steward Observatory, University of Arizona; and the Mayall telescope, Kitt Peak National Observatory, NOIRLab. NOIRLab is operated by the Association of Universities for Research in Astronomy (AURA) under a cooperative agreement with the National Science Foundation. Pipeline processing and analyses of the data were supported by NOIRLab and the Lawrence Berkeley National Laboratory. Legacy Surveys also uses data products from the Near-Earth Object Wide-field Infrared Survey Explorer (NEOWISE), a project of the Jet Propulsion Laboratory/California Institute of Technology, funded by the National Aeronautics and Space Administration. Legacy Surveys was supported by: the Director, Office of Science, Office of High Energy Physics of the U.S. Department of Energy; the National Energy Research Scientific Computing Center, a DOE Office of Science User Facility; the U.S. National Science Foundation, Division of Astronomical Sciences; the National Astronomical Observatories of China, the Chinese Academy of Sciences and the Chinese National Natural Science Foundation. LBNL is managed by the Regents of the University of California under contract to the U.S. Department of Energy. The complete acknowledgments can be found at https://www.legacysurvey.org/.

The authors are honored to be permitted to conduct scientific research on Iolkam Du'ag (Kitt Peak), a mountain with particular significance to the Tohono O'odham Nation.

Now that we know it's important, there are many ways we can refine the estimate and use it to calibrate DESI's measurement.

The best way we can improve it is by using the real distances to galaxies, which DESI is gathering right now!

DATA AVAILABILITY

All data from the DESI Legacy Imaging Survey is publicly available at legacysurvey.org. AbacusSummit simulations are publicly available at abacusnbody.org. Code for projecting ellipsoids and generating light profiles can be found at github.com/cmlamman/ellipse_alignment.

REFERENCES

WE DIDN'T START FROM SCRATCH

This project is built upon the work and ideas of others, and is part of an ongoing scientific conversation

Abareshi B., et al., 2022, Technical report, Overview of the Instrumentation for the Dark Energy Spectroscopic Instrument, https://ui.adsabs.harvard.edu/abs/2022arXiv220510939A. Lawrence Berkeley National Laboratory, https://ui.adsabs.harvard.edu/abs/2022arXiv220510939A

Anderson L., et al., 2014, Monthly Notices of the Royal Astronomical Society, 441, 24

Binney J., 1985, Monthly Notices of the Royal Astronomical Society, 212, 767

Catelan P., Porciani C., 2001, Monthly Notices of the Royal Astronomical Society, ...

Collaboration P., et al., 2020, Astronomy and Astrophysics, 641, A6

DESI Collaboration et al., 2016, Technical report, The DESI Experiment Part II: Instrument Design, https://ui.adsabs.harvard.edu/abs/2016arXiv161100037D. Lawrence Berkeley National Laboratory, https://ui.adsabs.harvard.edu/abs/2016arXiv161100037D

Dey A., et al., 2019, The Astronomical Journal, 157, 168

Gatti M., et al., 2021, Monthly Notices of the Royal Astronomical Society, 504, 4312

Gendzwill D. J., Stauffer M. R., 1981, Journal of the International Association for Mathematical Geology, 13, 135

Hadzhiyska B., Eisenstein D., Bose S., Garrison L. H., Maksimova N., 2021, Monthly Notices of the Royal Astronomical Society, 509, 501

Hernquist L., 1990, The Astrophysical Journal, 356, 359

Hirata C. M., 2009, Monthly Notices of the Royal Astronomical Society, 399, 1074

Hirata C. M., Seljak U., 2004, Physical Review D, 70, 063526

Hirata C. M., Mandelbaum R., Ishak M., Seljak U., Nichol R., Pimbblet K. A., Ross N. P., Wake D., 2007, Monthly Notices of the Royal Astronomical Society, 381, 1197

Hogg D. W., Lang D., 2013, Publications of the Astronomical Society of the Pacific, 125, 719

Jackson J. C., 1972, Monthly Notices of the Royal Astronomical Society, 156, 1P

Kaiser N., 1987, Monthly Notices of the Royal Astronomical Society, 227, 1

Kitanidis E., et al., 2020, Monthly Notices of the Royal Astronomical Society, 496, 2262

Kong H., et al., 2020, Monthly Notices of the Royal Astronomical Society, 499, 3943

Landy S. D., Szalay A. S., 1993, The Astrophysical Journal, 412, 64

Lang D., Hogg D. W., Mykytyn D., 2016, Astrophysics Source Code Lib p. ascl:1604.008

Maksimova N. A., Garrison L. H., Eisenstein D. J., Hadzhiyska B., Satterthwaite T. P., 2021, Monthly Notices of the Royal Astro Society, 508, 4017

Martens D., Hirata C. M., Ross A. J., Fang X., 2018, Monthly Notic Royal Astronomical Society, 478, 711

Obuljen A., Percival W. J., Dalal N., 2020, Journal of Cosmology troparticle Physics, 2020, 058

Padilla N. D., Strauss M. A., 2008, Monthly Notices of the Royal Astronomical Society, 388, 1321

Singh S., Mandelbaum R., More S., 2015, Monthly Astronomical Society, 450, 2195

Singh S., Yu B., Seljak U., 2021, Monthly Notices of the Roy Society, 501, 4167

Tenneti A., Mandelbaum R., Di Matteo T., Feng Y., Khandai N., 2014, Monthly Notices of the Royal Astronomical Society, 441, 470

Troxel M. A., Ishak M., 2015, Physics Reports, 558, 1

Zhou R., et al., 2021, Monthly Notices of the Royal Astronomical Society, 501, 3309

To learn more about DESI,
check out desi.lbl.gov

If you've gotten this far, CONGRATULATIONS! I hope my notes made it easier to digest this paper. If you're a scientist, I would love to read similar notes on one of your papers :)

I made this in power point using the XKCD font:
https://github.com/ipython/xkcd-font

?

What??
You're still reading?

APPENDIX A: PROJECTION OF TRIAXIAL ELLIPSOIDS

This section details how we obtained the axis ratios and orientations of projected triaxial ellipsoids for our mock [illegible]gs. We adapted the method derived in Gendzwill & Stauffer (1981) to project ellipsoids onto the celestial sphere.

Welcome to the part of my
paper I'm most proud of.

We denote the 3 ellipsoidal axis lengths as λ_j, $j = 1, 2, 3$. We then define the diagonal matrix $\mathbf{\Gamma}$ such that $\Gamma_{ij} = \delta_{ij}\lambda_j^{-2}$, where δ is a Kronecker delta. We normalize the corresponding axis directions $\vec{s}_j$ and organize them as rows of a matrix $\mathbf{S}$, so that S_{ij} is the j^{th} component of the i^{th} vector. We are projecting along the $\hat{x}$ unit vector direction, here denoted as component 1, onto the $\hat{y}-\hat{z}$ plane.

We define the column vector $\vec{m}$ as

$$\vec{m} = \left(\hat{x}^T\mathbf{S}^T\mathbf{\Gamma}\mathbf{S}\hat{x}\right)^{-1}\hat{x}^T\mathbf{S}^T\mathbf{\Gamma}\mathbf{S} \tag{A1}$$

Turns out, projecting a triaxial
ellipsoid (i.e. figuring out what
shape a 3D galaxy will have on the
sky) is NOT as simple as you may
think.

where the pre-factor adopts the normalization that $\vec{m}\cdot\hat{x} = 1$. We then compute vectors $\vec{u}$ and $\vec{v}$ with elements $u_j = \hat{y}\cdot(\vec{m}\times\vec{s}_j)$ and $v_j = \hat{z}\cdot(\vec{m}\times\vec{s}_j)$, written alternatively as

$$u_j = m_1 S_{j3} - m_3 S_{j1} \tag{A2}$$
$$v_j = m_1 S_{j2} - m_2 S_{j1} \tag{A3}$$

We use these to compute the scalars $A = \vec{u}^T\mathbf{\Gamma}\vec{u}$, $B = \vec{u}^T\mathbf{\Gamma}\vec{v}$, and $C = \vec{v}^T\mathbf{\Gamma}\vec{v}$.

The orientation angle of the projected ellipse's primary axis, measured in the $+\hat{y}$ direction from $\hat{z}$ is

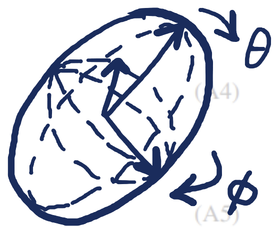

$$\tan 2\theta = \frac{-2B}{A-C} \tag{A4}$$

I found a great reference in
a *geology* paper from 1981!
They needed to know what
shape a 3D rock would have
when you cut through it.

And the minor and major axis lengths of the ellipse, b and a are given as:

$$\frac{1}{a^2} = \frac{A+C}{2} + \frac{A-C}{2\cos 2\theta} \tag{A5}$$
$$\frac{1}{b^2} = A + C - \frac{1}{a^2} \tag{A6}$$

To project the shapes on the sky, we rotated the original ellipsoid eigenvectors using the object's right ascension and declination, so that $\hat{x}$ lay along the LOS. This results in the axis lengths and orientation angle measured East of North for each halo. A function which performs these operations is available here: github.com/cmlamman/ellipse_alignment

We adapted their method for galaxies, and
present it here in a very clean way (I hope)!

APPENDIX B: EXPANDED DERIVATIONS

B1 Shape-Density Correlation

Starting from Equation 16, we can continue the computation as:

$$w_\times(R) = \frac{\tau}{L}\int dz \int \frac{d^3q}{(2\pi)^3}\left[\frac{q^2/3 - q_y^2}{q^2}\right] e^{-i\vec{q}\cdot\vec{x}}\Big|_{\vec{x}=0}\int \frac{d^3k}{(2\pi)^3}\, e^{i\vec{k}\cdot\vec{r}}\Big|_{\vec{r}=(R,0,z)}\left\langle\tilde{\rho}^*(\vec{q})\tilde{\rho}(\vec{k})\right\rangle \tag{B1}$$

$$= \frac{\tau}{L}\int dz \int \frac{d^3k}{(2\pi)^3}\left[\frac{k^2}{3} - k_y^2\right] k^{-2}P(k)\, e^{i\vec{k}\cdot\vec{r}}\Big|_{\vec{r}=(R,0,z)}. \tag{B2}$$

Next, the integral over z creates $\int dz\, \exp(ik_z z) = (2\pi)\delta^D(k_z)$. We denote the space of (k_x, k_y) as $\vec{K}$, and similarly $\vec{R}$ as (x, y). So we have

$$w_\times(R) = \frac{\tau}{L}\int \frac{d^2K}{(2\pi)^2}\left(\frac{K^2}{3} - K_y^2\right)K^{-2}P(K)e^{iK_xR}. \tag{B3}$$

To simplify this, we introduce

$$\Phi(\vec{R}) = \int \frac{d^2K}{(2\pi)^2}\frac{P(K)}{K^2}e^{i\vec{K}\cdot\vec{R}}, \tag{B4}$$

which in turn implies

$$w_\times(R) = \frac{\tau}{3L}\left(2\partial_y^2 - \partial_x^2\right)\Phi(\vec{R})\Big|_{\vec{R}=R\hat{x}}. \tag{B5}$$

$\Phi(\vec{R})$ is isotropic, and can be simplified to a Hankel transform

$$\Phi(R) = \int \frac{K\,dK}{2\pi}\frac{P(K)}{K^2}J_0(KR) \tag{B6}$$

with J_0 being the Bessel function. For a general function $f(R)$, we have $\partial^2 f/\partial x^2 = \partial^2 f/\partial R^2$ and $\partial^2 f/\partial y^2 = (1/R)\partial f/\partial R$. So we have

$$w_\times(R) = \frac{\tau}{3L}\left(\frac{2}{R}\partial_R - \partial_R^2\right)\Phi(R) = \frac{\tau}{3L}R^2\frac{d}{dR}\left[\frac{1}{R^2}\Psi(R)\right] \tag{B7}$$

where we introduce

$$\Psi(R) = -\frac{d\Phi}{dR} = \int \frac{K\,dK}{2\pi}\frac{P(K)}{K}J_1(KR), \tag{B8}$$

using $dJ_0(x)/dx = J_1(x)$.

B2 Shape - ξ_2 Correlation

Details of the derivation of Equation 22

Using $L_2(\mu) = (3/2)\mu^2 - (1/2)$,

$$q_z^2 - \frac{q^2}{3} = q^2\left(\mu_q^2 - \frac{1}{3}\right) = \frac{2q^2}{3}L_2(\mu_q) \tag{B9}$$

for a 3-d vector $\vec{q}$, and $L_\ell = \sqrt{4\pi/(2\ell+1)}Y_{\ell 0}$. We note that

$$\frac{T_{zz}}{2} = \frac{1}{3}\int \frac{d^3k}{(2\pi)^3}L_2(\mu_k)\tilde{\rho}(\vec{k})e^{i\vec{k}\cdot\vec{r}}. \tag{B10}$$

Finally, we have the expansion of a plane wave into spherical harmonics and spherical Bessel functions:

$$e^{i\vec{q}\cdot\vec{r}} = 4\pi\sum_{\ell m} i^\ell j_\ell(qr)Y^*_{\ell m}(\hat{q})Y_{\ell m}(\hat{r}). \tag{B11}$$

We then compute $\langle\epsilon_{zz}Q(r)\rangle$ as

$$\langle\epsilon_{zz}Q(r)\rangle = 5\tau\int\frac{d^3q}{(2\pi)^3}\frac{1}{3}L_2(\hat{q})\int\frac{d^2\hat{r}}{4\pi}L_2(\hat{r})\int\frac{d^3k}{(2\pi)^3}e^{i\vec{q}\cdot\vec{r}}\left\langle\tilde{\rho}^*(\vec{q})\tilde{\rho}(\vec{k})\right\rangle \tag{B12}$$

Converting to power, doing the $\vec{k}$ integral, and expanding the plane wave yields

$$\langle\epsilon_{zz}Q(r)\rangle = \frac{5\tau}{3}\int\frac{q^2dq}{2\pi^2}P(q)\int\frac{d^2\hat{q}}{4\pi}L_2(\hat{q})\int\frac{d^2\hat{r}}{4\pi}L_2(\hat{r})4\pi\sum_{\ell m}i^\ell j_\ell(qr)Y^*_{\ell m}(\hat{q})Y_{\ell m}(\hat{r}). \tag{B13}$$

We then can do the two angular integrals, yielding the simpler form:

$$\langle\epsilon_{zz}Q(r)\rangle = -\frac{\tau}{3}\int\frac{q^2dq}{2\pi^2}P(q)j_2(qr). \tag{B14}$$

This paper has been typeset from a TEX/LATEX file prepared by the author.

Alright, this is actually the end.